European Journal of Medical Research

RESEARCH

Open Access

CBL-mediated AQP1 ubiquitination aggravates kidney-yang deficiency syndrome by promoting lipid metabolism dysregulation

Yifei Wang[1†], Jun Yuan[1†], Wenfang He[1], Nan Yang[1], Lanjun Fu[1*] and Juan Jin[1*]

Abstract

Objective Kidney-Yang Deficiency Syndrome (KYDS) is associated with lipid metabolism dysregulation. This study aimed to investigate the effect of casitas B-lineage lymphoma (CBL)-mediated aquaporin 1 (AQP1) ubiquitination on KYDS.

Methods The KYDS rat model was induced via intraperitoneal injection of hydrocortisone. Body weight, body temperature, sperm motility, serum hormone levels, organ indices, and histopathological changes of rats were evaluated. AQP1 was knocked down to detect the effect of AQP1 on lipid metabolism in KYDS rats. Immunofluorescence and immunoprecipitation were used to verify the relationship between CBL and AQP1, and CBL knockdown KYDS rats were constructed to test the effect of CBL on AQP1 ubiquitination.

Results AQP1 expression was downregulated in KYDS rats. Knockdown of the AQP1 gene in KYDS rats resulted in decreased body weight, body temperature, sperm motility, and testicular index, along with increased renal index. It also resulted in changes of serum hormone levels and exacerbated pathologic changes. Additionally, AQP1 knockdown further suppressed lipid accumulation in KYDS rats, as evidenced by reductions in lipid droplets and the expression of lipid synthesis proteins. Intriguingly, elevated expression of CBL was observed in KYDS, and its knockdown inhibited the ubiquitin-mediated degradation of AQP1. The inhibition of CBL in KYDS improved lipid metabolism dysregulation, thereby ameliorating KYDS.

Conclusion CBL-mediated AQP1 ubiquitination aggravates KYDS by promoting lipid metabolism dysregulation, offering promising insights for targeted therapeutic interventions.

Keywords Kidney-Yang Deficiency Syndrome, Aquaporin 1, Ubiquitination, Casitas B-lineage lymphoma, Lipid metabolism

Introduction

Kidney-Yang Deficiency Syndrome (KYDS) is a common metabolic disorder characterized by neuroendocrine dysfunction, and its pathogenesis involves hypothalamic-pituitary-target gland axis dysfunction [1]. The primary symptoms of KYDS include reduced sexual function, frequent urination, and soreness and weakness in the waist and knees [2]. The incidence of KYDS in China is gradually increasing, greatly reducing people's quality of life. Exploring the underlying regulatory mechanisms of

†Yifei Wang and Jun Yuan are co-first authors and contributed equally to this work.

*Correspondence:
Lanjun Fu
fulanjun2013@163.com
Juan Jin
20233004@zcmu.edu.cn
[1] Department of Nephrology, the First Affiliated Hospital of Zhejiang Chinese Medical University (Zhejiang Provincial Hospital of Chinese Medicine), Hangzhou, Zhejiang 310000, China

© The Author(s) 2025. **Open Access** This article is licensed under a Creative Commons Attribution-NonCommercial-NoDerivatives 4.0 International License, which permits any non-commercial use, sharing, distribution and reproduction in any medium or format, as long as you give appropriate credit to the original author(s) and the source, provide a link to the Creative Commons licence, and indicate if you modified the licensed material. You do not have permission under this licence to share adapted material derived from this article or parts of it. The images or other third party material in this article are included in the article's Creative Commons licence, unless indicated otherwise in a credit line to the material. If material is not included in the article's Creative Commons licence and your intended use is not permitted by statutory regulation or exceeds the permitted use, you will need to obtain permission directly from the copyright holder. To view a copy of this licence, visit http://creativecommons.org/licenses/by-nc-nd/4.0/.

KYDS has thus become a top priority in contemporary research.

Disruption of lipid metabolism could potentially influence the structure and function of the kidneys, including the carnitine reabsorption process in renal tubules [3–5]. Lu et al. have revealed abnormal lipid metabolic activity in KYDS [1]. Previous research indicates that Gushudan can retain the intestinal microbiota of KYDS rats, improving fatty acid metabolism to exert its therapeutic effects [6]. However, the regulatory mechanisms of lipid metabolism in KYDS remain unclear.

Aquaporins (AQPs) are water channel proteins present in various tissues, and play an important role in regulating water transport, lipid metabolism, and glycolysis of cells [7]. AQP1, especially abundant in the kidneys, plays a pivotal role in the process of urine concentration [8]. Its main function is to facilitate the movement of water molecules across the cell membrane in response to osmotic gradients [9, 10]. The ubiquitination of AQP1 could potentially disrupt the stability and function of AQP1, further inhibiting water reabsorption in the kidneys [11]. Shen Qi Wan was found to promote rat renal proximal tubular cell migration by increasing AQP1 expression in KYDS [12]. However, the precise role of AQP1 in KYDS and its relationship with lipid metabolism remain unclear.

Casitas B-lineage Lymphoma(CBL), ubiquitously expressed ubiquitin E3 ligase, plays a critical role in maintaining the homeostasis and activation state of numerous signaling molecules [13]. CBL-mediated ubiquitination can destabilize target proteins, thereby inhibiting their function [14]. For example, the overexpression of CBL alleviates endothelial dysfunction in diabetes by enhancing the ubiquitination of janus tyrosine kinase 2 (JAK2) [15]. In HCV-infected cells, CD2AP enhances the ubiquitination of IRS1 and increases the level of lipid droplets by interacting with CBL [16]. Our analysis has identified AQP1 as a possible novel substrate for ubiquitin ligase CBL. Bioinformatic analysis indicates AQP1 downregulation and CBL upregulation in KYDS samples, highlighting their interaction with genes related to lipid metabolism (Supplementary Fig. 1 A–B). Thus, we hypothesize that CBL might promote dysregulated lipid metabolism to aggravate KYDS by enhancing AQP1 ubiquitination.

The rat is a common animal model for KYDS [17]. We established a rat KYDS model to go deeper into the role and mechanism of CBL-mediated AQP1 ubiquitination

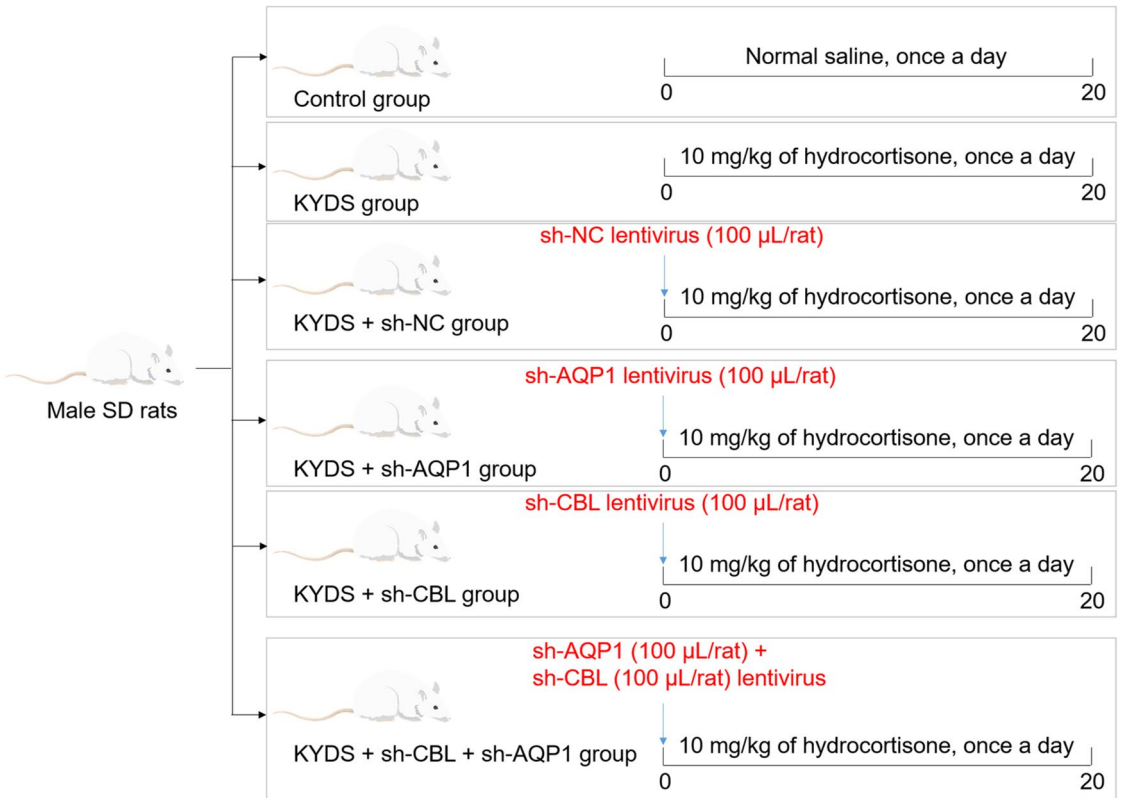

Fig. 1 Flow chart of animal experiment. The administration method for normal saline and hydrocortisone was via intraperitoneal injection, while that for lentivirus was via tail vein injection

in KYDS. This study delves into the role of CBL-mediated AQP1 ubiquitination in dysregulated lipid metabolism associated with KYDS. By uncovering the molecular mechanisms of KYDS, the investigation identifies potential therapeutic targets, offering insights into the diagnosis and treatment of KYDS.

Materials and methods

Animal model construction

Male Sprague-Dawley (SD) rats (250 ± 20 g, 6 weeks old, the College of Veterinary Medicine at Yangzhou University) were housed under standard laboratory conditions, with a 12-h light/dark cycle, and temperature and humidity maintained at 23–27 °C and 30%–70%, respectively. After a one-week acclimatization period, the rats were randomly divided into six groups ($n = 6$ per group): Control, KYDS, KYDS + sh-NC (negative control), KYDS + sh-AQP1, KYDS + sh-CBL, and KYDS + sh-CBL + sh-AQP1. Rats in the KYDS, KYDS + sh-NC, KYDS + sh-AQP1, KYDS + sh-CBL, and KYDS + sh-CBL + sh-AQP1 groups were intraperitoneally injected with 10 mg/kg of hydrocortisone once daily for 20 consecutive days to induce a KYDS model [18]. The control group rats received an equal volume of normal saline. Before modeling, to knockdown AQP1 and/or CBL expression, rats in the KYDS + sh-AQP1, KYDS + sh-CBL, and KYDS + sh-CBL + sh-AQP1 groups were intravenously injected via tail vein with AQP1 and/or CBL interfering lentivirus (4×10^7 TU/mL, 100 μL; AQP1: 5'- GGT CAA GCT CAG CAG TCA A-3'; CBL: 5'-GGT TTA TAT TGT TAG AAT A-3'). Rats in the KYDS + sh-NC group received an equivalent volume of the sh-NC lentivirus. At the end of the treatment period, rats were euthanized via intraperitoneal injection of 50 mg/kg sodium pentobarbital, followed by cervical dislocation. All efforts were approved by Yangzhou University's Animal Ethics Committee (202308007). The workflow is shown in Fig. 1.

Observation of physiological parameters

Weight: the body weight of the rats was measured and recorded every two days for a continuous period of 20 days after the model construction.

Body temperature: their body temperature was measured and recorded before euthanizing the rats in each group.

Sperm motility: after intraperitoneal injection of sodium pentobarbital, the epididymis of each rat was extracted. It was placed in 8 mL of normal saline, cut into pieces to ensure even distribution, and incubated in a 37 °C water bath for 10 min. The suspension was then filtered, and an additional 8 mL of normal saline was added to create a sperm suspension. Under a microscope, one drop of the sperm suspension was observed to assess the motility of 100 sperm cells. According to the World Health Organization (WHO) manual, sperm motility is classified into four grades: A (fast forward movement), B (slow forward movement), C (nonforward movement), and D (no movement). The proportion of A + B grade sperm was calculated.

Organ indices: the kidneys and testes of the rats in each group were weighed. The organ index of each organ was calculated using the following formula: organ index = (organ weight/body weight) × 100%.

Serum cytokine: after intraperitoneal injection of sodium pentobarbital, 5 mL of abdominal aortic blood was collected from each rat (rats were allowed free access to water 12 h prior to blood collection). After 2 h of incubation, the blood samples were centrifuged at 3000 rpm for 10 min, and the serum was collected. The concentrations of cyclic adenosine monophosphate (cAMP; mlbio, Shanghai, China; ml002907), cyclic guanosine monophosphate (cGMP; mlbio; ml003133), gonadotropin-releasing hormone (GnRH; Shanghai WESTANG, Shanghai, China; MY567), luteinizing hormone (LH; mlbio; ml064293), follicle-stimulating hormone (FSH; mlbio; ml059034), testosterone (T; Abcam, UK; ab285350), estradiol (E2; Abcam; ab285285), corticosterone (CORT; Abcam; ab108821), corticotropin releasing hormone (CRH; mlbio; ml003041), adrenocorticotrophic hormone (ACTH; mlbio; ml002875), and tetraiodothyronine (T4; Abcam; ab285258) in the serum were determined using ELISA kits.

Hematoxylin and eosin (HE) staining

Tissue sections with a thickness of 5 μm were prepared using formalin fixation. Sections were stained by hematoxylin solution (Beyotime, Shanghai, China; C0105S), which was used to stain nuclei. The excess color was washed away before an appropriate amount of eosin solution was added for staining the cytoplasm and extracellular matrix. After washing away the excess color, the sections were dehydrated through a series of alcohol baths, starting with 80% ethanol, followed by 95%, and ending with 100% ethanol. This was followed by the clearing of the sections using xylene to make them transparent. Lastly, the sections were sealed with a suitable amount of a resinous mounting medium and covered with a glass coverslip. The sections were observed under a microscope (Olympus, Japan) for subsequent experimental analysis.

Red oil O staining

Kidney and testicular tissues were fixed with formalin and cryosectioned, ensuring that the tissue was cut to an appropriate thickness of 8 μm. Sections were placed on a dry glass slide and cover the Oil Red O solution

(Beyotime; C0158S) evenly on the section so that it was completely infiltrated. After staining for 20 min, Oil Red O solution was removed and washed the sections with wash solution. Afterwards, the sections were sealed and observed using a microscope (Olympus).

Immunohistochemistry

Following fixation with cold acetone, the sections of kidney and testicular tissues were treated with 3% H_2O_2 for 20 min to quench endogenous peroxidase activity. The sections were then blocked with normal goat serum for 15 min. The primary antibody anti-SREBP-1 (1:100; Abcam, UK; ab28481) was applied to the kidney sections, and anti-3β-HSD (1:200; Bioss, China; bs-3906R) was incubated with the testicular sections overnight at 4 °C. This was followed by an incubation with a secondary antibody (Abcam; ab6721) at a 1:2000 dilution for 30 min. 3,3'-Diaminobenzidine was used for color development, with the reaction monitored closely to avoid overstaining. Sections were mounted and analyzed under a light microscope (Olympus, Japan).

Cell culture

The HEK293T cells (American Type Culture Collection, Manassas, VA, USA) were cultured in RPMI 1640 medium (Gibco, Carlsbad, CA, USA) supplemented with 10% fetal bovine serum and 1% penicillin/streptomycin in a carbon dioxide incubator at 37 °C, and the medium was replaced every 2–3 days.

Cell transfection

We engineered sh-NC, sh-CBL, oe-NC, and oe-CBL constructs and packaged them into lentiviruses utilizing a third-generation packaging system (pMDLg/pRRE, pRSV-Rev, and pVSV-G). HEK293T cells were seeded in a 6-well plate at a density of 2×10^5 cells/mL. When the cell confluence reached 70–90%, the lentivirus, which expresses either overexpression (oe-) or knockdown (sh-) CBL, was thawed on ice, diluted in complete culture medium to a titer of 1×10^8 TU/mL, and 20 μL of the lentivirus was added to each well. After 18 h of lentiviral infection, the medium was replaced with fresh complete culture medium. Stable cell lines expressing the target gene were obtained after 48 h of infection.

Immunoprecipitation detection

The HEK293T cells were lysed using a non-denaturing lysis buffer (Thermo Fisher Scientific, MA, USA), complemented with protease and phosphatase inhibitors (Roche, Basel, Switzerland). The cell lysates were incubated with anti-AQP1 (1:30) overnight at 4 °C with gentle shaking. The following day, protein A/G PLUS-Agarose beads (Santa Cruz Biotechnology, TX, USA) were added to each sample and incubated at 4 °C for an additional 2 h with gentle shaking. The beads were then collected by centrifugation and washed three times with RIPA buffer to remove non-specifically bound proteins. Finally, the immunoprecipitated protein complexes were eluted by boiling the beads in Laemmli Sample Buffer (Bio-Rad) for 5 min. These eluted samples were then analyzed by Western blot.

Western blot

Protein samples were prepared from tissues and cells using RIPA lysis buffer (Beyotime). Protein concentrations were determined using a BCA Protein Assay Kit (Beyotime). Equal amounts of protein (25 μg) were separated by sodium dodecyl sulfate-polyacrylamide gel electrophoresis (Bio-Rad, CA, USA) and transferred onto polyvinylidene fluoride membranes. Membranes were blocked with 5% non-fat milk for 1 h at room temperature. Subsequently, membranes were incubated with primary antibodies overnight at 4 °C. After washing, membranes were incubated with HRP-conjugated secondary antibodies (1:2000; Abcam; ab6721) for 1 h at room temperature. Signals were imaged on a ChemiDoc XRS+ system (Bio-Rad) and the densitometry of bands was analyzed using Image Lab software (Bio-Rad). Antibodies used in this study are SIRT1 (1:1000; DF6033), E-cadherin (1:1000; AF0131), Vimentin (1:1000; AF7013), CBL (1:1000; AF6225), AQP1 (1:1000; AF5231) were purchased from Affinity Biosciences (OH, USA); SERBP1 (1:1000), Ubiquitin (1:1000; ab134953), and GAPDH (1:2500; ab9485) were purchased from Abcam.

Immunofluorescence detection

The distribution and expression of CBL and AQP1 in cells were detected by immunofluorescence. Initially, cells were fixed with a 3% formaldehyde solution at room temperature for 15 min, followed by membrane permeabilization using 1% Triton-X 100 for 10 min. To mitigate non-specific antibody interactions, cells were then incubated in a 3% BSA blocking solution at room temperature for 30 min. Primary antibodies against CBL and AQP1, diluted to a 1:100 ratio in the blocking solution, were applied to the samples and incubated in a humidity-controlled chamber at 4 °C overnight. A fluorescence detection step involved adding a mixture of secondary antibody (diluted 1:500) and DAPI to the cells, followed by a 30-min incubation in the dark at room temperature. Finally, the prepared coverslips were mounted onto glass microscope slides using a fluorescence-quenching mounting medium and were sealed with nail polish to prevent dehydration. Imaging was conducted using laser confocal scanning microscopy (Perkin Elmer, MA, USA).

Quantitative real-time PCR (qRT-PCR) assay

The experiment was carried out following the methods described in previous research [19]. Primer sequences are as follow: CBL, forward 5'-GCC AGT ACC TCC CAC ACT TC-3', reverse 5'-TCT GCT GGT CGC AAT CAC AT-3'; and GAPDH, forward 5'-TGT GGG CAT CAA TGG ATT TGG-3', reverse 5'-ACA CCA TGT ATT CCG GGT CAA T-3'.

Statistical analysis

Statistical analyses were performed using GraphPad 7.0 (GraphPad, Inc., CA, USA), with data presented as means ± standard deviations. The Shapiro-Wilks test was used to test the normality of data, and Levene's test was applied to assess the homogeneity of variance. The statistical significance of differences was assessed using a one-way ANOVA, followed by Tukey's test. A value of $P < 0.05$ was considered to be statistically significant.

Results

AQP1 knockdown promotes lipid metabolism dysregulation to aggravate KYDS

To investigate the regulatory role of AQP1 in KYDS, we knocked down AQP1 in the KYDS rat model. As shown in Fig. 2A–C, KYDS rats exhibited significant declines in body weight, growth rate, body temperature, and sperm motility compared to controls ($P < 0.01$). AQP1 knockdown exacerbated these declines ($P < 0.05$). Moreover, the testicular index was diminished, while the kidney index was elevated in KYDS rats, with these differences becoming more pronounced upon AQP1 knockdown ($P < 0.05$; Fig. 2D). Furthermore, KYDS rats displayed serum hormone level alterations: decreases in ACTH, cAMP, CORT, T, and T4, and increases in cGMP, CRH, E2, FSH, GnRH, and LH ($P < 0.01$). These changes intensified with sh-AQP1 transfection ($P < 0.01$; Fig. 2E). HE staining showed that the kidney tissues of KYDS rats showed shrunken renal tubules, thickened basement membranes, increased connective tissue hyperplasia, and heightened inflammatory cell infiltration. Testicular tissues highlighted disarray in sperm cell arrangement within the seminiferous tubules, reduced interstitial cells and spermatozoa, and some detached sperm cells. AQP1 knockdown accentuated these pathological changes (Fig. 2F).

Additionally, Oil Red O staining indicated diminished lipid accumulation in the KYDS rat kidney and testicular tissues, with this reduction being more profound in the AQP1-knockdown KYDS group (Fig. 3A), suggesting that knockdown AQP1 promotes lipid metabolism dysregulation in KYDS. Immunohistochemical analysis of SREBP-1 (a key transcription factor regulating lipid synthesis) expression in kidneys and 3β-HSD (a key enzyme for steroid hormone synthesis) expression in testicular tissues was performed. Results revealed significantly lower expression levels in all experimental groups compared to the control group. The KYDS + sh-AQP1 group displayed significantly lower SREBP-1 and 3β-HSD expression compared to the KYDS + sh-NC group (Fig. 3B). In addition, the expression of AQP1, SREBP-1, and E-cadherin (epithelial-mesenchymal transition marker) was downregulated, and the expression of SIRT1 (negative regulator of lipogenesis) and Vimentin (epithelial-mesenchymal transition marker) was upregulated in KYDS rat kidneys compared to controls ($P < 0.05$). These protein expression changes were enhanced by transfection with sh-AQP1 ($P < 0.05$; Fig. 3C).

CBL promotes AQP1 ubiquitination

In elucidating the molecular mechanism of AQP1 in KYDS, UbiBrowser (http://ubibrowser.ncpsb.org.cn) analysis revealed that AQP1 may be a novel substrate of ubiquitin ligase CBL. The expression of CBL was significantly increased compared to controls, while AQP1 level decreased in KYSD rat testicular tissues ($P < 0.05$). AQP1 expression was further decreased after AQP1 knockdown ($P < 0.01$; Fig. 4A). Immunofluorescence staining displayed co-localization of CBL and AQP1 on the cell membrane (Fig. 4B), and the interaction between CBL and AQP1 was confirmed through an immunoprecipitation assay (Fig. 4C).

To discern the regulatory function of CBL on AQP1 expression, AQP1 expression was assessed under conditions of CBL overexpression or knockdown ($P < 0.05$; Fig. 4D–E). CBL overexpression resulted in decreased AQP1 expression compared to the oe-NC group ($P < 0.05$). Conversely, CBL knockdown led to a significant increase in AQP1 expression levels compared to the sh-NC group ($P < 0.01$; Fig. 4E). Further exploration of the mechanism by which CBL regulates AQP1 revealed changes in AQP1 expression upon CBL knockdown, with or without MG132 (a proteasome inhibitor, 10 μM) treatment for 8 h. Specifically, a significant upregulation of AQP1 expression was observed in both the sh-NC + MG132 group (relative to the sh-NC group) and the sh-CBL + MG132 group (relative to the sh-CBL group) ($P < 0.01$; Fig. 4F). Additionally, with a protein synthesis inhibitor cycloheximide (CHX, 50 μg/mL) treatment, AQP1 protein degradation was more rapid in sh-NC transfected cells, while degradation was significantly slower in sh-CBL transfected cells ($P < 0.05$; Fig. 4G). Intriguingly, upon CBL knockdown, AQP1 ubiquitination was reduced ($P < 0.01$; Fig. 4H). These results suggest that CBL, functioning as a specific E3 ubiquitin ligase for AQP1, promotes the ubiquitination modification of AQP1.

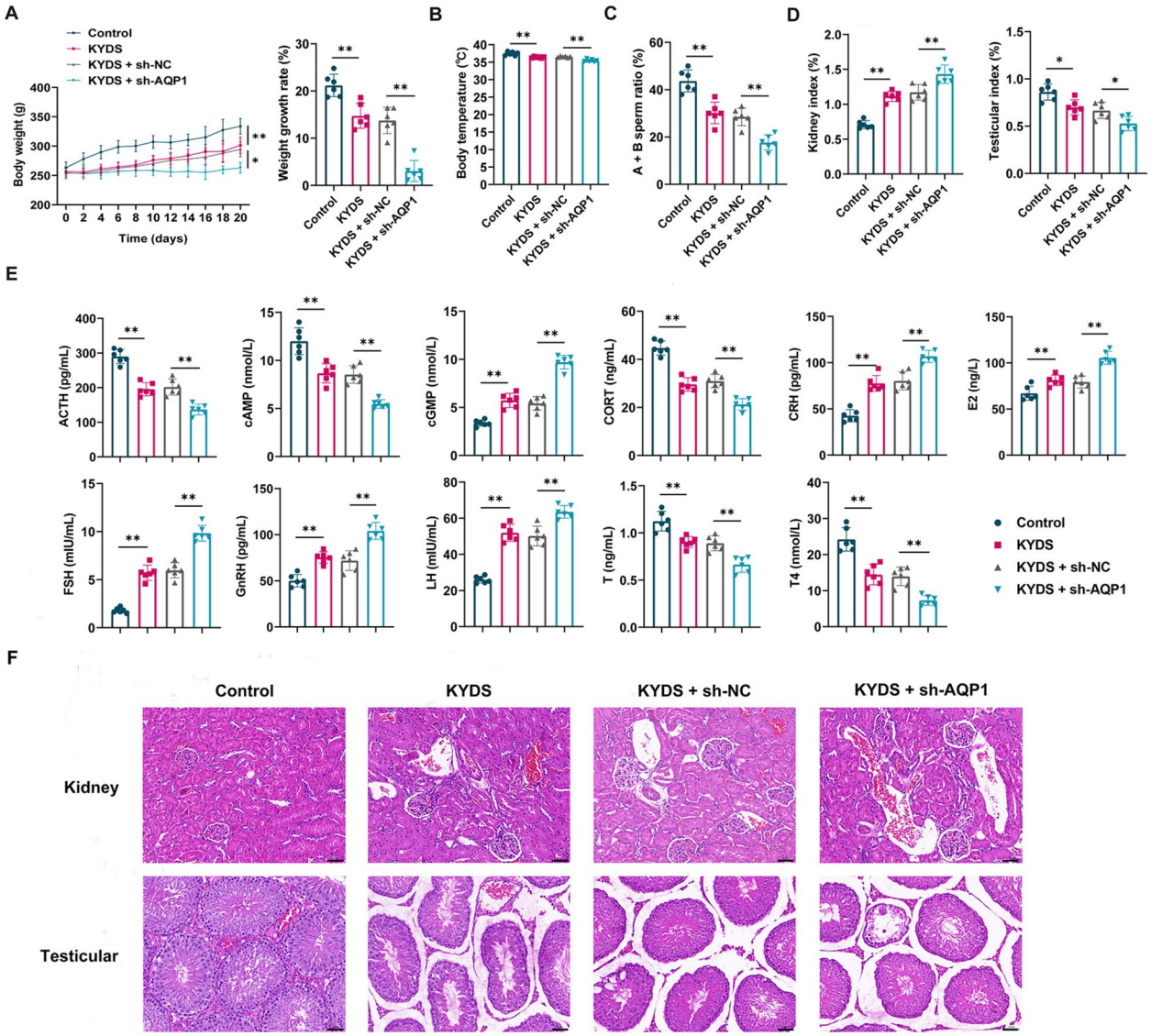

Fig. 2 Aquaporin 1 (AQP1) knockdown exacerbates the symptom of Kidney-Yang Deficiency Syndrome (KYDS). **A** Body weight and growth rate of rats in the control, KYDS, KYDS + sh-NC, and KYDS + sh-AQP1 groups. **B** Comparison of body temperature measurements between groups. **C** Sperm motility of rats in each group. **D** Organ index evaluation for kidneys and testes across experimental groups. **E** Serum levels of adrenocorticotrophic hormone (ACTH), cyclic adenosine monophosphate (cAMP), cyclic guanosine monophosphate (cGMP), corticosterone (CORT), corticotropin releasing hormone (CRH), estradiol (E2), follicle-stimulating hormone (FSH), gonadotropin-releasing hormone (GnRH), luteinizing hormone (LH), testosterone (T), and tetraiodothyronine (T4) in the control, KYDS, KYDS + sh-NC, and KYDS + sh-AQP1 groups. **F** Histopathological changes in kidney and testes across groups, as visualized through Hematoxylin and eosin staining (400×); scale bar: 50 μm. *$P < 0.05$, **$P < 0.01$

CBL knockdown alleviates lipid metabolism disorders in KYDS by inhibiting AQP1 ubiquitination

To determine the role of CBL-mediated AQP1 deubiquitination in KYDS, a KYDS model was constructed. Firstly, CBL expression was enhanced in the kidney and testicular tissues of KYDS rats relative to controls ($P < 0.05$). However, upon transfection with sh-CBL, this expression diminished ($P < 0.01$). Intriguingly, in KYDS rats with sh-CBL transfection, AQP1 expression increased, a trend which was reversed with sh-AQP1 transfection ($P < 0.01$; Fig. 5A and B). Sequential investigations revealed that metrics such as body weight, weight growth rate, body temperature, and sperm motility augmented in KYDS rats under CBL knockdown (Fig. 5C–E). In assessments of organ indices, the indices of testes rose, while those of the kidneys

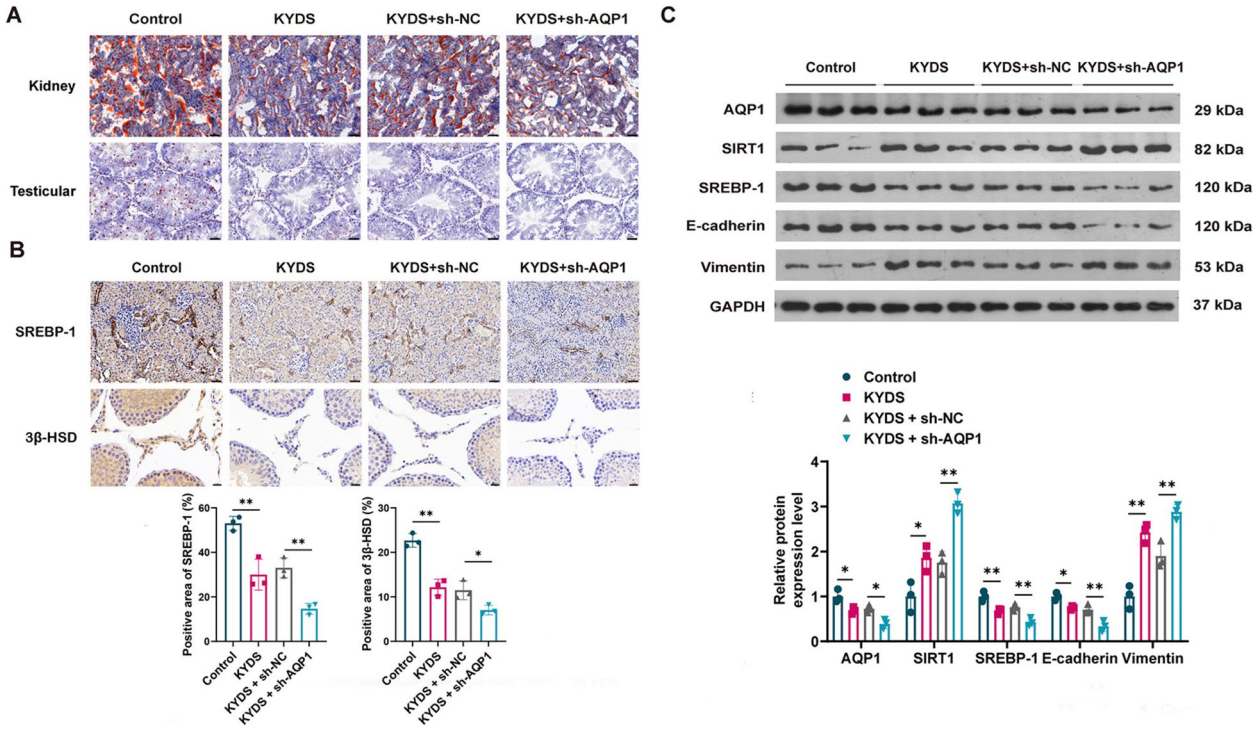

Fig. 3 AQP1 knockdown promotes lipid metabolism dysregulation in KYDS. **A** Oil Red O staining demonstrating lipid accumulation variations in kidney and testicular tissues across groups (400×); scale bar: 50 μm. **B** Immunohistochemical analysis showing SREBP-1 expression in kidneys and 3β-HSD expression in testicular tissues across different groups (400×); scale bar: 50 μm. **C** Western blot bands representing protein expression levels of AQP1, SIRT1, SREBP-1, E-cadherin, and Vimentin in kidneys in different experimental setups. **P* < 0.05, ***P* < 0.01

decreased in sh-CBL-treated KYDS rats compared to the KYDS group ($P < 0.05$; Fig. 5F). AQP1 knockdown partially counteracted these alterations. ELISA assays further demonstrated that the KYDS + sh-CBL group exhibited heightened levels of ACTH and T and reduced serum concentrations of cGMP, GnRH, and LH compared to the KYDS group ($P < 0.01$). Suppressing AQP1 moderated these variables ($P < 0.05$; Fig. 5G). Histological assessments showed renal and testicular improvements in KYDS rats with CBL suppression, which were negated when AQP1 expression was simultaneously inhibited (Fig. 5H).

Oil Red O staining evidenced a significant increase in lipid droplets within the renal and testicular tissues of the KYDS + sh-CBL group compared to the KYDS + sh-NC group. Interestingly, the KYDS + sh-CBL + sh-AQP1 group exhibited even fewer lipid reserves than the KYDS + sh-CBL group (Fig. 6A). Immunohistochemistry exhibited that CBL knockdown significantly increased 3β-HSD level in KYDS rat testicular tissue, which was decreased when AQP1 expression was simultaneously downregulated (Fig. 6B). Furthermore, in KYDS + sh-CBL rats, there was a decrease in SIRT1 and Vimentin expression, whereas SREBP-1 and E-cadherin expression was amplified, compared to KYDS-sh-NC rats ($P < 0.01$). These expression patterns were reversed with sh-AQP1 treatment ($P < 0.05$; Fig. 6C).

Discussion

In this study, histological results concerning AQP1/CBL were obtained through staining renal and testicular tissue sections and protein sample analysis. Moreover, we investigated the roles of AQP1 and CBL in the development of KYDS and their interplay in regulating each other. Our research findings revealed that AQP1 knockdown exacerbated adverse physiological changes and dysfunction of lipid metabolism in KYDS. CBL knockdown attenuated the ubiquitination process of AQP1, which further suppressed the dysregulation of lipid metabolism to improve KYDS.

Kidney-Yang Deficiency is a metabolic disorder characterized by impotence, enuresis, and frequent urination [20]. In this study, the testicular index decreased, while the renal index increased in KYDS rats, with obvious pathological changes, suggesting the occurrence of KYDS in these rats. Previous research has revealed that the cAMP/cGMP ratio, CRH, and ACTH levels were reduced, while triglycerides and liver lipids were increased in KYDS mice [20]. Similarly, our results showed abnormal serum hormone levels and lipid

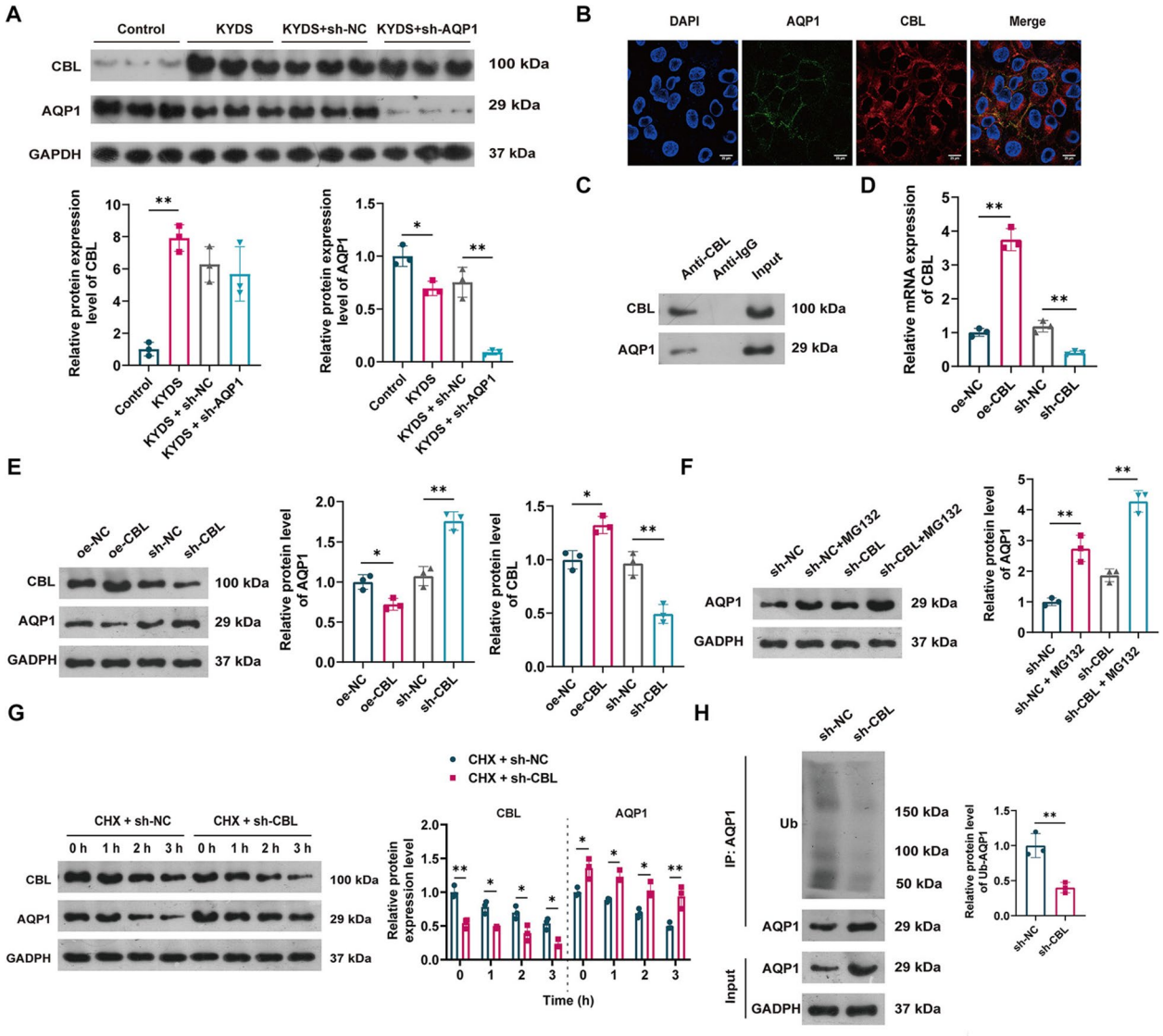

Fig. 4 CBL promotes AQP1 ubiquitination. **A** Western blot bands representing protein expression levels of Casitas B-lineage lymphoma (CBL) and AQP1 in testicular tissues in different experimental setups. **B** Immunofluorescence images indicating co-localization of CBL and AQP1 on the cell membrane (400×); scale bar: 25 μm. **C** Immunoprecipitation assay highlighting the interaction between CBL and AQP1. **D** mRNA expression levels of CBL with CBL overexpression or knockdown. E, Protein expression levels of CBL and AQP1 with CBL overexpression or knockdown. **F** AQP1 protein levels post CBL knockdown with or without MG132 treatment. **G**, AQP1 degradation kinetics upon cycloheximide (CHX) treatment in CBL-knockdown and control cells. **H** Ubiquitination levels of AQP1 upon CBL knockdown. *$P < 0.05$, **$P < 0.01$

metabolism dysregulation in KYDS rats. Lipid metabolism disorder may play a key role in promoting KYDS development.

AQP1, as a membrane protein regulating water transport, has multiple cytological functions such as transport, uptake, secretion and cell migration, lipid metabolism, neurotransmission, and volumetric regulation [7, 21–24]. AQP1 plays an important role in renal water transport and participates in the physiological processes of primary urinary filtration and reabsorption. For example, studies have shown that the expression level of AQP1 is low in renal tubular epithelial cells of patients with KYDS, and that AQP1 knockout may disrupt renal water balance and osmoregulation, thereby aggravating symptoms associated with renal deficiency [12, 25, 26]. These findings suggest that AQP1 plays a crucial role in kidney function. In this study, AQP1 knockdown led to a pronounced decline in body weight, body temperature, and sperm motility, accompanied by significant changes in serum hormone levels and exacerbated tissue damage in the kidney and

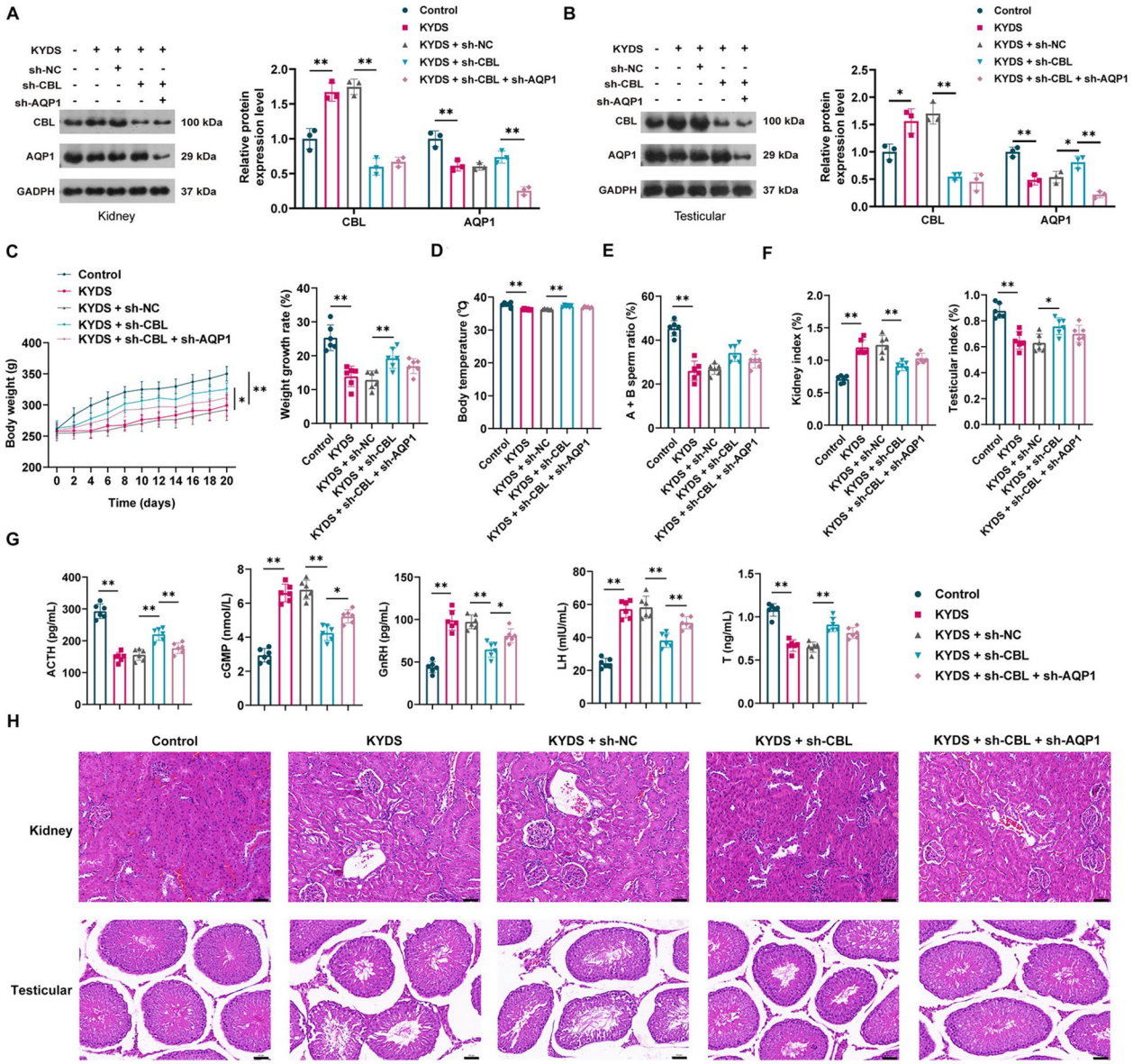

Fig. 5 CBL knockdown alleviates the symptoms of KYDS via suppressing AQP1 ubiquitination. **A** Western blot bands showing CBL and AQP1 expression levels in kidneys. **B** Western blot bands showing CBL and AQP1 expression levels in testicular tissues. **C** Body weight variations and growth rate in rats upon suppressing CBL and AQP1 levels. **D** Temperature fluctuations across groups. **E** Sperm motility comparisons in the presence of CBL and/or AQP1 knockdown. **F** Organ indices variations of kidneys and testes upon inhibiting CBL and AQP1 expression. **G** Serum concentrations of ACTH, cGMP, GnRH, LH, and T upon CBL knockdown and subsequent AQP1 intervention. **H** Histological kidney and testicular tissue images from KYDS rats with CBL knockdown, with and without AQP1 suppression (400×); scale bar: 50 μm.*$P < 0.05$, **$P < 0.01$

testicular tissues, promoting KYDS. Furthermore, extensive studies have demonstrated that lipid accumulation is involved in the development of renal dysfunction-related diseases such as chronic kidney disease, acute lung injury, and lipoprotein glomerulopathy [27, 28]. This study found a decrease in lipid accumulation in the kidney and testicular tissues of KYDS rats with AQP1 knockdown. These results suggest that AQP1 knockdown impairs lipid metabolism in KYDS, thus positioning AQP1 as a potential therapeutic target for KYDS.

The CBL family comprises two important members, C-CBL and CBL-B, both of which function as E3 ubiquitin ligases. C-CBL and CBL-B participate in metabolic homeostasis by increasing the protein levels and stability of STRT2 [29]. In cells infected with HCV, CD2AP enhances IRS1 ubiquitination and lipid droplet levels

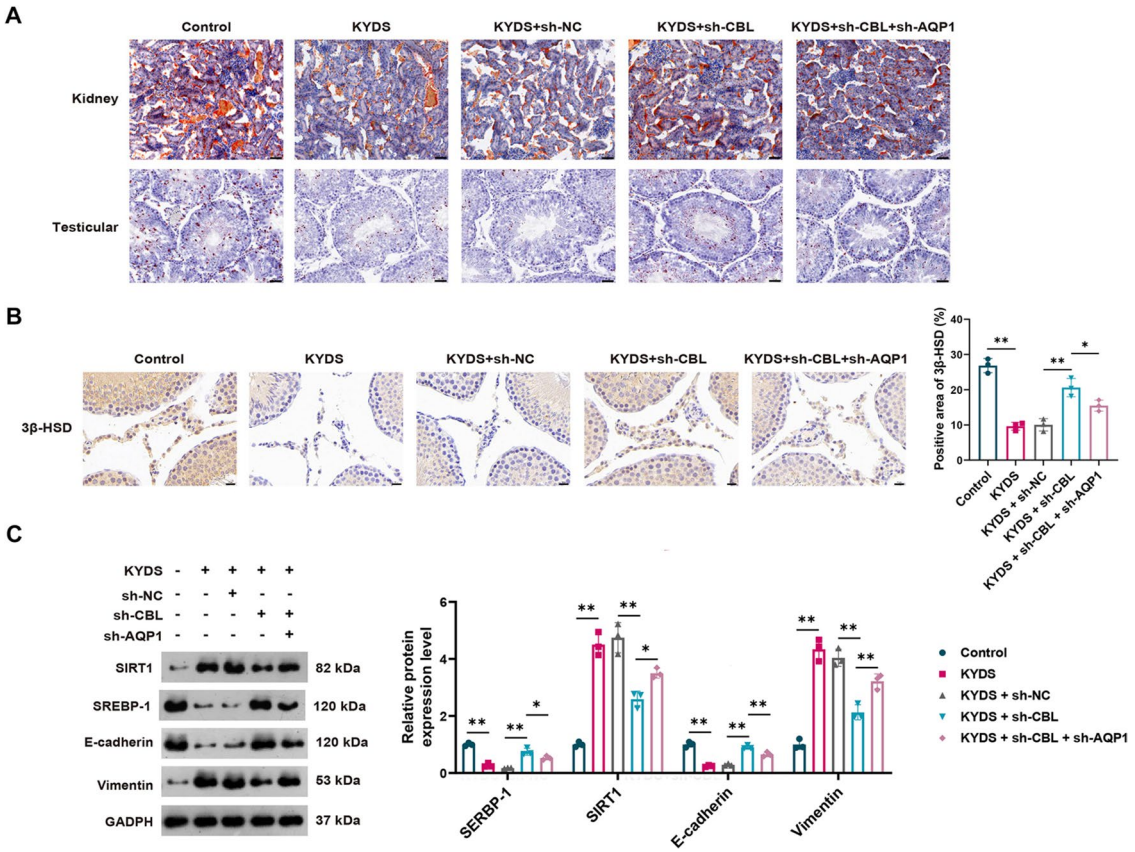

Fig. 6 CBL knockdown mitigates lipid metabolism disorders in KYDS via suppressing AQP1 ubiquitination. **A** Oil Red O staining of kidney and testicular tissues from various groups (400×); scale bar: 50 μm. **B** Immunohistochemical analysis showing 3β-HSD expression in testicular tissues across different groups (400×); scale bar: 50 μm. **C** Western blot bands showing expression trends of SIRT1, SREBP-1, E-cadherin, and Vimentin upon CBL and AQP1 knockdown. *$P < 0.05$, **$P < 0.01$

by interacting with CBL [16]. These studies suggest that CBL, acting as an E3 ubiquitin ligase, could potentially disrupt lipid metabolic homeostasis. In our research, we found that CBL promotes the ubiquitin-mediated degradation of AQP1, and concurrently aggravates lipid metabolic dysregulation in KYDS rats.

However, this study has some limitations. Although hydrocortisone-induced KYDS models are commonly used, there may be differences in the pathological mechanisms compared to actual clinical KYDS cases. Moreover, AQP1 was not overexpressed in the KYDS model, making it difficult to directly evaluate its therapeutic potential. In addition, further clinical trials are needed to verify the role of CBL-mediated AQP1 ubiquitination in KYDS.

Conclusion

Our study revealed that AQP1 and CBL are pivotal factors in pathophysiology of KYDS. Notably, CBL-mediated AQP1 ubiquitination promotes lipid metabolism dysregulation in KYDS. These findings offer new diagnostic markers and therapeutic avenues for KYDS.

Supplementary Information

The online version contains supplementary material available at https://doi.org/10.1186/s40001-025-02743-9.

Additional file1

Additional file2

Acknowledgements

We would like to thank Yangzhou University for providing the platform for animal experiments and monitoring the whole process.

Author contributions

Conceptualization: Yifei Wang, Lanjun Fu, Juan Jin. Data curation: Yifei Wang, Jun Yuan, Wenfang He, Juan Jin. Formal analysis: Yifei Wang, Jun Yuan, Lanjun Fu, Wenfang He. Funding acquisition: Lanjun Fu. Investigation: Yifei Wang, Wenfang He, Nan Yang. Project administration: Juan Jin. Resources: Jun Yuan, Wenfang He. Supervision: Lanjun Fu, Juan Jin. Validation: Wenfang He, Nan Yang. Visualization: Yifei Wang, Jun Yuan, Nan Yang. Writing – original draft: Yifei Wang, Jun Yuan. Writing – review & editing: Lanjun Fu, Juan Jin.

Funding

This work was supported by Science Research Fund Project of Zhejiang Chinese Medical University [grant numbers 2020ZG37 and 2022 FSYYZY01].

Available of data and materials
No datasets were generated or analysed during the current study.

Declarations

Ethics statement
All efforts were approved by Yangzhou University's Animal Ethics Committee (202308007).

Competing interests
The authors declare no competing interests.

Received: 2 April 2025 Accepted: 28 May 2025
Published online: 06 June 2025

References

1. Lu Q, Zhang J, Xin L, Lou Y, Qin F, Zhao L, et al. Integrated gas chromatography-mass spectrometry and ultra-high-performance liquid chromatography-mass spectrometry renal metabolomics and lipidomics deciphered the metabolic regulation mechanism of Gushudan on kidney-yang-deficiency-syndrome rats. J Sep Sci. 2023;46(13):e2300124.
2. Wang K, Li J, Zheng X, Xu J, Wang Z, Li S, et al. The pharmacological effects and safety of the raw and prepared folium of Epimedium brevicornu Maxim. on improving kidney-yang deficiency syndrome and sexual dysfunction. Front Pharmacol. 2023;14:1233468.
3. Giardini E, Moore D, Sadlier D, Godson C, Brennan E. The dual role of lipids in chronic kidney disease: Pathogenic culprits and therapeutic allies. Atherosclerosis. 2024;398:118615.
4. Bignon Y, Wigger L, Ansermet C, Weger BD, Lagarrigue S, Centeno G, et al. Multiomics reveals multilevel control of renal and systemic metabolism by the renal tubular circadian clock. J Clin Invest. 2023;133(8):e167133.
5. Pan S, Li Z, Wang Y, Liang L, Liu F, Qiao Y, et al. A Comprehensive Weighted Gene Co-expression Network Analysis Uncovers Potential Targets in Diabetic Kidney Disease. J Transl Int Med. 2022;10(4):359–368.
6. Tong L, Feng Q, Lu Q, Zhang J, Xiong Z. Combined (1)H NMR fecal metabolomics and 16S rRNA gene sequencing to reveal the protective effects of Gushudan on kidney-yang-deficiency-syndrome rats via gut-kidney axis. J Pharm Biomed Anal. 2022;217:114843.
7. Li M, He M, Xu F, Guan Y, Tian J, Wan Z, et al. Abnormal expression and the significant prognostic value of aquaporins in clear cell renal cell carcinoma. PLoS One. 2022;17(3):e0264553.
8. Huang P, Hansen JS, Saba KH, Bergman A, Negoita F, Gourdon P, et al. Aquaglyceroporins and orthodox aquaporins in human adipocytes. Biochim Biophys Acta Biomembr. 2022;1864(1):183795.
9. Tradtrantip L, Verkman AS. Aquaporin gene therapy for disorders of cholestasis? Hepatology. 2016;64(2):344–346.
10. Rodriguez RA, Liang H, Chen LY, Plascencia-Villa G, Perry G. Single-channel permeability and glycerol affinity of human aquaglyceroporin AQP3. Biochim Biophys Acta Biomembr. 2019;1861(4):768–775.
11. Pohl M, Shan Q, Petsch T, Styp-Rekowska B, Matthey P, Bleich M, et al. Short-term functional adaptation of aquaporin-1 surface expression in the proximal tubule, a component of glomerulotubular balance. J Am Soc Nephrol. 2015;26(6):1269–1278.
12. He Y, Bao YT, Chen HS, Chen YT, Zhou XJ, Yang YX, et al. The Effect of Shen Qi Wan Medicated Serum on NRK-52E Cells Proliferation and Migration by Targeting Aquaporin 1 (AQP1). Med Sci Monit. 2020;26:e922943.
13. Yang X, Hao D, He B. The Regulation of E3 Ubiquitin Ligases Cbl and its Cross-talking in Bone Homeostasis. Curr Stem Cell Res Ther. 2021;16(6):683–687.
14. Liyasova MS, Ma K, Voeller D, Ryan PE, Chen J, Klevit RE, et al. Cbl interacts with multiple E2s in vitro and in cells. PLoS One. 2019;14(5):e0216967.
15. Jin Q, Lin L, Zhao T, Yao X, Teng Y, Zhang D, et al. Overexpression of E3 ubiquitin ligase Cbl attenuates endothelial dysfunction in diabetes mellitus by inhibiting the JAK2/STAT4 signaling and Runx3-mediated H3K4me3. J Transl Med. 2021;19:1–16.
16. Zhang H, Zhang C, Tang H, Gao S, Sun F, Yang Y, et al. CD2-Associated Protein Contributes to Hepatitis C, Virus Propagation and Steatosis by Disrupting Insulin Signaling. Hepatology. 2018;68(5):1710–1725.
17. Lu Q, Zhang J, Xin L, Lou Y, Qin F, Zhao L, et al. Integrated gas chromatography-mass spectrometry and ultra-high-performance liquid chromatography-mass spectrometry renal metabolomics and lipidomics deciphered the metabolic regulation mechanism of Gushudan on kidney-yang-deficiency-syndrome rats. J Separ Sci. 2023;46(13):e2300124.
18. Tan Y, Liu X, Lu C, He X, Li J, Xiao C, et al. Metabolic profiling reveals therapeutic biomarkers of processed Aconitum Carmichaeli Debx in treating hydrocortisone induced Kidney-Yang deficiency syndrome rats. J Ethnopharmacol. 2014;152(3):585–593.
19. Zhao W, Geng D, Li S, Chen Z, Sun M. LncRNA HOTAIR influences cell growth, migration, invasion, and apoptosis via the miR-20a-5p/HMGA2 axis in breast cancer. Cancer Med. 2018;7(3):842–855.
20. Zheng X, Li S, Wang K, Wang Z, Li J, Yang Q, et al. Comparing the pharmacological effects of the prepared folium of Epimedium brevicornu Maxim. and Epimedium sagittatum Maxim. on kidney-Yang deficiency syndrome and liver injury complications. Fitoterapia. 2024;176:106006.
21. Su W, Cao R, Zhang XY, Guan Y. Aquaporins in the kidney: physiology and pathophysiology. Am J Physiol Renal Physiol. 2020;318(1):F193–F203.
22. Caglayan C, Kandemir FM, Yildirim S, Kucukler S, Eser G. Rutin protects mercuric chloride-induced nephrotoxicity via targeting of aquaporin 1 level, oxidative stress, apoptosis and inflammation in rats. J Trace Elem Med Biol. 2019;54:69–78.
23. Liu M, Sun Y, Xu M, Yu X, Zhang Y, Huang S, et al. Role of mitochondrial oxidative stress in modulating the expressions of aquaporins in obstructive kidney disease. Am J Physiol Renal Physiol. 2018;314(4):F658–F666.
24. Li B, Liu C, Tang K, Dong X, Xue L, Su G, et al. Aquaporin-1 attenuates macrophage-mediated inflammatory responses by inhibiting p38 mitogen-activated protein kinase activation in lipopolysaccharide-induced acute kidney injury. Inflamm Res. 2019;68(12):1035–1047.
25. Verkman AS. Aquaporins in endothelia. Kidney Int. 2006;69(7):1120–1123.
26. Hua Y, Ying X, Qian Y, Liu H, Lan Y, Xie A, et al. Physiological and pathological impact of AQP1 knockout in mice. Biosci Rep. 2019;39(5):BSR20182303.
27. Yoon H, Shaw JL, Haigis MC, Greka A. Lipid metabolism in sickness and in health: Emerging regulators of lipotoxicity. Mol Cell. 2021;81(18):3708–3730.
28. Bugarski M, Ghazi S, Polesel M, Martins JR, Hall AM. Changes in NAD and Lipid Metabolism Drive Acidosis-Induced Acute Kidney Injury. J Am Soc Nephrol. 2021;32(2):342–356.
29. Choi YH, Kim H, Han Y, Jin YH, Lee KY. Cbl regulates the activity of SIRT2. Biochem Biophys Res Commun. 2014;453(3):557–562.

Publisher's Note

Springer Nature remains neutral with regard to jurisdictional claims in published maps and institutional affiliations.